Jyväskylän yliopiston julkaisuarkisto
Jyväskylä University Digital Archive

UNIVERSITY OF JYVÄSKYLÄ

This is an electronic reprint of the original article.
This reprint *may differ* from the original in pagination and typographic detail.

Author(s): Lahtinen, Tanja; Hulkko, Eero; Sokołowska, Karolina; Tero, Tiia-Riikka; Saarnio, Ville; Lindgren, Johan; Pettersson, Mika; Häkkinen, Hannu; Lehtovaara, Lauri

Title: Covalently linked multimers of gold nanoclusters Au102(p-MBA)44 and Au250(p-MBA)n

Year: 2016

Version:

Please cite the original version:

Lahtinen, T., Hulkko, E., Sokołowska, K., Tero, T.-R., Saarnio, V., Lindgren, J., Pettersson, M., Häkkinen, H., & Lehtovaara, L. (2016). Covalently linked multimers of gold nanoclusters Au102(p-MBA)44 and Au250(p-MBA)n. Nanoscale, 8(44), 18665-18674. https://doi.org/10.1039/C6NR05267C

All material supplied via JYX is protected by copyright and other intellectual property rights, and duplication or sale of all or part of any of the repository collections is not permitted, except that material may be duplicated by you for your research use or educational purposes in electronic or print form. You must obtain permission for any other use. Electronic or print copies may not be offered, whether for sale or otherwise to anyone who is not an authorised user.

Please do not adjust margins

Journal Name

ARTICLE

Covalently linked multimers of gold nanoclusters Au_{102}(*p*-MBA)$_{44}$ and $Au_{\sim 250}$(*p*-MBA)$_n$

Received 00th January 20xx,
Accepted 00th January 20xx

DOI: 10.1039/x0xx00000x

www.rsc.org/

Tanja Lahtinen[a‡], Eero Hulkko[a‡], Karolina Sokołowska[a], Tiia-Riikka Tero[a], Ville Saarnio[a], Johan Lindgren[a], Mika Pettersson[a*], Hannu Häkkinen[a,b*], Lauri Lehtovaara[a*]

We present synthesis, separation, and characterization of covalently-bound multimers of *para*-mercaptobenzoicacid (*p*-MBA) protected gold nanoclusters. The multimers were synthesized by performing a ligand-exchange reaction of pre-characterized Au_{102}(*p*-MBA)$_{44}$ nanocluster with biphenyl-4,4'-dithiol (BPDT). The reaction products were separated using gel electrophoresis yielding several distinct bands. The bands were analyzed with transmission electron microscopy (TEM) revealing monomer, dimer, and trimer fractions of the nanocluster. TEM analysis of dimers in combination with molecular dynamics simulations suggest that the nanoclusters are covalently bound via a disulfide bridge between BPDT molecules. The linking chemistry is not specific to Au_{102}(*p*-MBA)$_{44}$. The same approach yields multimers also for a larger monodisperse *p*-MBA –protected cluster of approximately 250 gold atoms, $Au_{\sim 250}$(*p*-MBA)$_n$. Whereas the Au_{102}(*p*-MBA)$_{44}$ is not plasmonic, $Au_{\sim 250}$(*p*-MBA)$_n$ nanocluster supports localized surface plasmon resonance (LSPR) at 530 nm. Multimers of $Au_{\sim 250}$(*p*-MBA)$_n$ exhibit additional transitions in their UV-vis spectrum at 630 nm and at 810 nm, indicating presence of hybridized LSPR modes. Well-defined structure and relatively small size make these systems excellent candidates for connecting *ab initio* theoretical studies and experimental quantum plasmonics. Moreover, our work opens new possibilities in controlled synthesis of advanced monodisperse nanocluster superstructures.

Introduction

Nanoparticles (NPs) and their superstructures have attracted a lot of interest in fundamental research as well as in nanotechnological applications. The main reason is that physicochemical properties of nanoparticles are often strikingly different from their bulk counterparts and depend on composition, size, shape, and internal structure of the nanoparticles.[1,2] The properties of superstructures are influenced by their immediate surroundings including other nanoparticles. For example, optical spectrum of metal nanoparticles is dominated by localized surface plasmon (LSPR) that hybridizes with LSPRs of other nearby NPs.[3] The hybridization leads to formation of "hotspots" in between of the NPs, where electromagnetic field intensity increases orders of magnitudes. This had led to many applications. For example, nanoparticle dimers can act as nanoscale distance probes because of their sensitivity to interparticle spacing.[4,5] The field enhancement has been employed, for example, in surface enhanced Raman spectroscopy[6], where sensitivity has reached single molecule level[7].

There exist several different approaches to fabricate NP assemblies and superstructures. The most straightforward is to simply aggregate NPs.[8] More stable structures can be achieved with polymer or silica encasing[9,10] or templating polymer layers[11]. Lithography has been extensively used to fabricate plasmonic nanoparticle assemblies in a controlled way.[12] However, for several applications, it would be desirable to have a controlled, wet-chemistry synthesis of superstructures. Successful wet-chemistry approaches based on self-assembly has been demonstrated, for example, with DNA-templating[13] and with several different molecular linkers[14-18].

Colloidal nanoparticles, in general, have a serious drawback from the chemical point-of-view. Their structure is not well-defined at the atomic level, and typical nanoparticle synthesis produces a polydisperse sample of different sizes, shapes, and surface structures.[5] This seriously hinders synthesis of homogeneous NP superstructures, and experiments that require atomic-level control, for example, LSPR hybridization through molecular states, are extremely difficult to carry out reproducibly.

Monolayer protected clusters (MPC) are a special kind of NPs which have a well-defined atomic structure that can be accurately determined by mass spectrometry and by single-crystal X-ray diffraction similar to small molecules.[19] For

[a] *Department of Chemistry, Nanoscience Center, University of Jyväskylä, P.O. Box 35, 40014 Jyväskylä, Finland*
[b] *Department of Physics, Nanoscience Center, University of Jyväskylä, P.O. Box 35, 40014 Jyväskylä, Finland*
† These authors contributed equally.
* Emails: lauri.lehtovaara@jyu.fi, hannu.j.hakkinen@jyu.fi, mika.j.pettersson@jyu.fi

Electronic Supplementary Information (ESI) available: Details of syntheses and purification; additional images of PAGE runs; mass spectrum of Au_{102}(*p*-MBA)$_{44}$; ^{1}H NMR spectra of clusters; TEM analysis of cluster sizes; additional TEM images; core-to-core distance and angle distributions from simulations; additional multimer size statistics; additional UV-vis spectra for $Au_{\sim 250}$(*p*-MBA)$_n$ multimers and aggregates. See DOI: 10.1039/x0xx00000x

Please do not adjust margins

Please do not adjust margins

example, the crystal structure of *para*-mercaptobenzoicacid (*p*-MBA) protected $Au_{102}(p\text{-MBA})_{44}$ cluster, used in this work, shows a core of 79 gold atoms protected by 19 RS–Au–SR and two $Au_2(SR)_3$ units in a well-defined motif.[20,21]

The atomically precise structures of MPC have enabled accurate studies of their chemistry. $Au_{102}(p\text{-MBA})_{44}$ and other MPCs are known to have preferred sites for ligand exchange reactions, i.e., specific ligands are exchanged with higher probability than others.[22,23] A well-defined structure with unequal ligand-exchange activities provides a basis for controlled synthesis of homogeneous NP superstructures.

An additional benefit of using MPCs to study fundamental aspects of NP superstructures is that depending on the size and shape of the metallic core, the electronic structure of MPC can change from discrete molecular-like energy levels[19], to semiconducting[24,25], and finally to metallic continuum[26,27]. The changes in the electronic structure are reflected to their physicochemical properties, for example, UV-vis spectrum changes from discrete peaks[19], to continuum[25], and finally to a spectrum with clear LSPR[26,27].

The well-defined atomic structure, preferred sites for ligand exchange, and possibility to approach nanoparticle limit from below in a controlled manner make MPCs excellent candidates for accurate studies of emergent properties in NP superstructures. Moreover, MPC superstructures and their possible MPC specific properties are inherently interesting themselves having potential applications in chemical sensing and biomedical imaging[28]. In this paper, we demonstrate a synthesis of small covalently linked MPC superstructures via ligand-exchange reaction where a biphenyl-4-4'-dithiol (BPDT) replaces a *p*-MBA ligand and creates a covalent disulfide bridge with another BPDT forming a MPC multimer. Furthermore, we show that emergence of plasmonic coupling can be studied using these MPC multimers. Previously, MPC dimers have been demonstrated using dynamic diglyme bonding[29], however, in our approach, dithiol-bridged MPCs form a covalently bound system.

The rest of the paper is structured as follows. We begin by describing synthesis and purification of $Au_{102}(p\text{-MBA})_{44}$ and $Au_{\sim 250}(p\text{-MBA})_n$ clusters and their BPDT linked multimers (see Fig. 1). Experimental analysis methods are described next, followed by computational methods. Results and discussion begins with characterization of $Au_{102}(p\text{-MBA})_{44}$ and analysis of $Au_{\sim 250}(p\text{-MBA})_n$ followed by analysis of their multimers. TEM analyses and molecular dynamics (MD) simulations are combined to explain the nature of the linking. In the last part of the paper, we focus on UV-vis spectroscopy of $Au_{\sim 250}(p\text{-MBA})_n$ multimers and interpretation of observed plasmonic features supported by density functional theory simulations.

Materials and methods

Materials

All reagents were commercial and used as received unless otherwise mentioned.

Synthesis of nanoclusters. Two different MPCs were synthesized to be used as starting material for the multimer synthesis. The smaller nanocluster, $Au_{102}(p\text{-MBA})_{44}$, has been extensively studied before.[20,21,22,24,25,30,31,32] We followed its previously reported synthesis given in Ref. 30. The larger nanocluster of approximately 250 gold atoms and unknown number of *p*-MBAs (labelled as $Au_{\sim 250}(p\text{-MBA})_n$) required a treatment of the initial $Au_x(p\text{-MBA})_y$, polymerization step at pH of ~11 before reduction that nucleates the growth of the metal core.[33] The syntheses of both sizes produced mg-quantities of material. Detailed description of the syntheses and purification are given in ESI.

Synthesis of nanocluster multimers. The ligand exchange reaction leading to multimers of $Au_{102}(p\text{-MBA})_{44}$ was carried out as follows. Stock solution of BPDT in THF was added to water solution of $Au_{102}(p\text{-MBA})_{44}$ (2:1 ratio of thiol groups vs. gold clusters) together with a few drops of NaOH. The reaction was quenched after 3.5 hours with isopropanol and 5 M NH_4OAc, and the resulting black precipitate was centrifuged. The supernatant was removed and the pellet was washed to remove any remaining free thiol residue. The ligand-exchange reaction of $Au_{\sim 250}(p\text{-MBA})_n$ was carried out the same way.

Separation of nanocluster multimers. Gel electrophoresis (PAGE) was used to separate reaction products of $Au_{102}(p\text{-MBA})_{44}$ and $Au_{\sim 250}(p\text{-MBA})_n$ multimer syntheses. Preparative PAGE was performed with a 2 mm thick gel. Different PAGE bands were mechanically cut from the acrylamide gel and dissolved separately in small amount of water. Clusters were

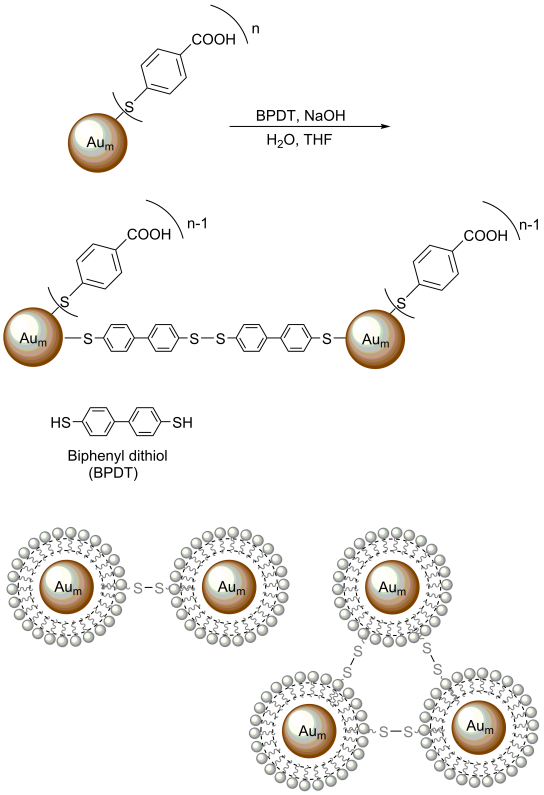

Fig. 1 Schematic representation of the ligand exchange and linking reaction. The scheme shows the molecular structure of biphenyl-4,4'-dithiol (BPDT), the covalent linking via two BPDTs as an example, and examples of dimeric and trimeric reaction products.

This journal is © The Royal Society of Chemistry 20xx

Please do not adjust margins

allowed to dissolve from the gel until significant coloration of the solution was observed (typically overnight). Solution was filtered through a centrifugal filter tube with a pore size of 0.22 µm (time: 60 s, speed: rcf = 1.0) to remove excess gel residues. The separation procedure was repeated for the separated bands to obtain higher purity for TEM imaging and optical absorption spectroscopy.

Experimental techniques

Polyacrylamide gel electrophoresis (PAGE). PAGE was run on a 15 or 20 % polyacrylamide gel (29:1 acrylamide:bisacrylamide) using 2X TBE run buffer in a Bio-Rad Mini-Protean Tetra System gel electrophoresis apparatus at 130 V.

Mass spectrometry (MS). Electrospray ionization mass spectrum of for $Au_{102}(p\text{-MBA})_{44}$ sample was measured at the University of Tokyo using a homemade TOF mass spectrometer with a similar procedure and parameters as previously reported in Ref. 31. The sample was dissolved in 50% (v/v) methanol/water containing 0.07% triethylamine.

Nuclear magnetic resonance (NMR) spectroscopy. ^{1}H NMR spectra were recorded on a Bruker Avance DRX 300 MHz (for $Au_{102}(p\text{-MBA})_{44}$) and 400 MHz (for $Au_{\sim 250}(p\text{-MBA})_n$) spectrometers.

UV-vis spectroscopy. Optical absorption measurements were done with Perkin Elmer Lambda 850 UV/Vis -spectrometer with 2 nm resolution.

Transmission electron microscopy (TEM) and image analysis. TEM samples were prepared by drop-casting 40 mL of dilute deionized water solution of linked nanoclusters on a glow discharged 400 mesh holey carbon copper grid (Ted-Pella ultrathin c). Solution was allowed to deposit for 15 min, after which excess sample was removed and grid was allowed to dry under vacuum overnight. Samples were imaged with 0.26 nm point resolution using JEOL JEM-1400HC TEM operated at 80 kV or 120 kV, equipped with bottom mounted 11 Megapixel CCD camera (Olympus SIS Quemesa).

TEM images were analyzed by semi-automatic procedure using in-house developed code. First, a blob detector filter was applied to TEM images, where the filter is difference of two Gaussians of widths σ and 2σ, and the value of σ depends on TEM magnification. After the automatic blob detection, the found particles were verified by a human, and any false positives were removed from further analysis. A 2D Gaussian function was fitted to a slightly smoothed TEM intensity around each detected and verified particle. Parameters of the fitted 2D Gaussians are stored for further analysis.

Exposure time for determining particle size was chosen not to saturate TEM images at the centers of particles. Size of the particle is reported as the average of the long and short axis full widths at half maximum (FWHM). For example, the crystal structure of $Au_{102}(p\text{-MBA})_{44}$ yields FWHM of 1.1 nm when each atom in the crystal structure is represented as a Gaussian charge distribution with intensity proportional to atomic number and width equal to 0.2 nm.

Computational methods

Molecular dynamics. The molecular dynamics (MD) simulations were performed with Gromacs 4.6.7[34] using periodic boundary conditions; leap-frog integrator with 2 fs time step; PME electrostatics with 1.0 nm cut-off and 0.12 nm grid spacing; and Lennard-Jones interaction with 1.0 nm cut-off and dispersion correction for energy and pressure. Simulated structures were placed in the center of cubic box and then solvated using TIP3P water model. Counterions (Na^+) were added, when needed, to neutralize the system. All simulations model NPT ensemble using velocity-rescale thermostat (reference temperature 298.15 K) and Berendsen barostat (reference pressure 1 bar). Total simulation time was 100 ns and sampling was started after 50 ns.

The force field parameters and charges for the gold-sulphur units, and deprotonated and protonated *p*-MBA ligands were obtained from Ref. 35. Existing force field parameters in AMBER12[36] were used for the BPDT molecule. The partial charges for BPDT were calculated using structures consisting of one, two, or three BPDT(s) capped by gold atoms at the ends. The ground state geometries of the structures were obtained using Gaussian09 software[37], B3LYP functional, def2-TZVP basis set, and W06 density fitting. The MD partial charges were calculated using Ambertools12[36] and RESP charge fitting procedure[38] in two stages with the charge of gold atoms set to zero. Radius of gold atoms was set to 0.17 nm. The partial charges can be found in ESI, Table S1. The force field parameters for BPDT linker molecules and for the atom types are listed in ESI, Table S2.

Dimeric $Au_{102}(p\text{-MBA})_{43}$ – $(BPDT)_n$ – $Au_{102}(p\text{-MBA})_{43}$ systems for molecular dynamics were constructed by replacing the *p*-MBA ligand labeled as "pMBA2" in Ref. 22 by a BPDT molecule. If structure contained more than one BPDT molecule, a disulfide bridge (RS–SR) was formed between BPDT molecules.

Density functional theory. The density functional theory (DFT) calculations were performed using GPAW 0.10.0[39], GPAW setups 0.9.11271 and PBE exchange-correlation functional. The initial structure for DFT simulations was taken from a MD simulation of deprotonated $Au_{102}(p\text{-MBA})_{43}$ – $(BPDT)_n$ – $Au_{102}(p\text{-MBA})_{43}$ where core-to-core distance was 3.4 nm. Both $Au_{102}(p\text{-MBA})_{43}$BPDT fragments were replaced by $Au_{314}(SH)_{96}$ from Malola et al.[40] in a such way that gold atoms in Au–SH–Au–SH–Au units of $Au_{314}(SH)_{96}$ were aligned with the respective gold atoms of Au–BPDT–Au–*p*-MBA–Au units of $Au_{102}(p\text{-MBA})_{43}$BPDT. The geometry of BPDT–BPDT linker was relaxed in a system where only Au–BPDT–Au–SH–Au units were included in the DFT calculation and all gold atoms were fixed.

Results and Discussion

Characterization of $Au_{102}(p\text{-MBA})_{44}$. The purified product of $Au_{102}(p\text{-MBA})_{44}$ synthesis was analyzed using PAGE, NMR, MS, TEM, and UV-vis. The synthesis product showed up as a single distinct band in PAGE (see Fig. 2, and ESI, Fig. S1) indicating a monodisperse MPC. MPC was identified as $Au_{102}(p\text{-MBA})_{44}$

Please do not adjust margins

based on its NMR and mass spectra. Electrospray ionization mass spectrum (see ESI, Fig. S2) shows peaks that correspond to different mass to charge ratios of partially deprotonated $Au_{102}(p\text{-MBA})_{44}$, and the NMR spectrum (see ESI, Fig. S3) reproduces the characteristic NMR fingerprint of $Au_{102}(p\text{-MBA})_{44}$.[32] UV-vis spectrum (see Fig. 3) and TEM diameter of 1.2 ± 0.3 nm (see ESI, Fig. S4) are also in agreement with previous studies.[20,25,31]

Analysis of $Au_{\sim 250}(p\text{-MBA})_n$. Previous studies have shown that MPCs in this size range have preferred sizes,[26,27,41] and the sizes appear as individual bands in PAGE.[41,42] Product of $Au_{\sim 250}(p\text{-MBA})_n$ synthesis forms a single distinct band in PAGE (see Fig. 2) indicating a monodisperse MPC. The band had lower mobility than $Au_{102}(p\text{-MBA})_{44}$ in the PAGE run indicating larger size (see ESI, Fig. S1A). This is consistent with TEM analysis, that yields 1.6 ± 0.3 nm core diameter (see ESI, Fig. S4). A rough estimate for the number of gold atoms can be obtained by assuming relatively similar shape and density for the two MPCs ($N_{102}/V_{102} = N_x/V_x$), and then scaling the number of gold atoms in $Au_{102}(p\text{-MBA})_{44}$ by their relative volume calculated from the estimated core diameters: $N_x = 102 \times (1.6 \text{ nm} / 1.2 \text{ nm})^3 \approx 240$.

UV-vis spectrum (see Fig. 3) shows a weak LSPR band at 530 ± 15 nm. Recent studies have shown that LSPR begins to appear when MPC has approximately 200 gold atoms and becomes stronger as the cluster size increases. Our spectrum is comparable to the reported spectra of 51 kDa[26], 45 kDa and 53 kDa clusters[27], with estimated number of gold atoms 250, 226, and 253, respectively. We label our larger MPC as $Au_{\sim 250}(p\text{-MBA})_n$ based on these TEM and UV-vis estimates.

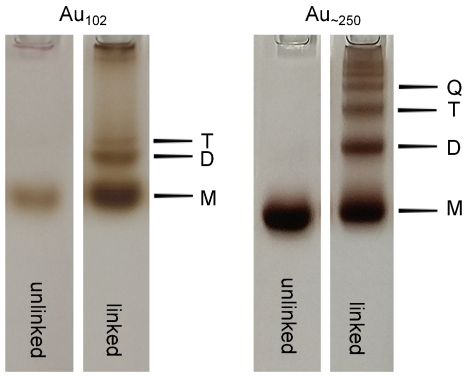

Fig. 2 PAGE bands of the $Au_{102}(p\text{-MBA})_{44}$ and $Au_{\sim 250}(p\text{-MBA})_n$ clusters and their linked multimers. $Au_{102}(p\text{-MBA})_{44}$ gels are from a different run than $Au_{\sim 250}(p\text{-MBA})_n$ gels, thus the run distances are not comparable. See ESI, Fig. S1A for samples in a same PAGE run.

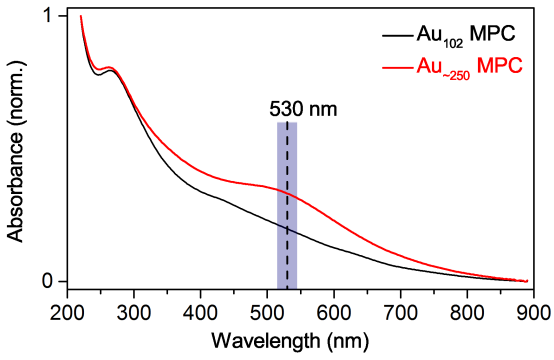

Fig. 3 Normalized UV-vis spectra of $Au_{102}(p\text{-MBA})_{44}$ (black) and $Au_{\sim 250}(p\text{-MBA})_n$ (red) clusters in H_2O. LSPR absorption maximum of $Au_{\sim 250}(p\text{-MBA})_n$ at 530 ± 15 nm is indicated with a dashed line.

Analysis of $Au_{102}(p\text{-MBA})_{44}$ multimers. Crude product from the $Au_{102}(p\text{-MBA})_{44}$ ligand-exchange synthesis was analyzed with UV-vis spectroscopy after purification (see Fig. 4). The spectrum essentially reproduces the spectrum of $Au_{102}(p\text{-MBA})_{44}$ in the visible region,[25] indicating that the cluster core remains intact in the reaction. New electronic transitions appear in the UV-region seen as spectral broadening of the ligand transitions, and the difference spectrum (see Fig. 4) reveals a new maximum in the linked clusters at 308 nm. The features closely resemble transitions of molecular BPDT measured in H_2O, but they are red-shifted. Although, optical coupling between the cores of $Au_{102}(p\text{-MBA})_{44}$ cannot be ruled out based on these observations, it is more likely that the observed feature originates from BPDT molecules bound to gold. Similar changes in the UV-vis spectrum has been reported before for diacetylene linked 1.1 nm AuNPs.[17]

The crude synthesis product was further analyzed by PAGE, where the sample separated to several distinct bands (see Fig. 1, and ESI, Fig. S1A). We label the three lowest bands as M, D, and T bands. The most intense and most mobile M band was aligned with the $Au_{102}(p\text{-MBA})_{44}$ reference band indicating that M band is unreacted $Au_{102}(p\text{-MBA})_{44}$ or monomeric $Au_{102}(p\text{-MBA})_{44-n}(BPDT)_n$. This was confirmed by TEM showing dominantly monomeric MPCs for the M band (see Fig. 5a, ESI Fig. S5). The D and T bands are clearly less mobile than the M band having shorter running distance than the $Au_{102}(p\text{-MBA})_{44}$ reference. TEM imaging of these bands shows dominantly dimers for the D band and a large fraction of trimers in T band (see Figs. 5b-c, ESI Figs. S5B-C).

TEM analysis of center-to-center distances in the D band yielded a distribution spanning from 1.8 nm up to 3.4 nm (see Fig. 5d). To gain insight into the nature of the bonding between multimers, we performed MD simulations of Au_{102}MPCs linked with one or more BPDT molecules. Atomistic models were constructed based on the known $Au_{102}(p\text{-MBA})_{44}$

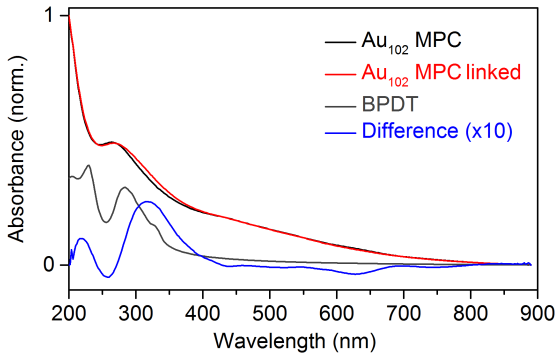

Fig. 4 Normalized UV-vis spectra of $Au_{102}(p\text{-MBA})_{44}$ before (black) and after (red) linking with BPDT in H_2O, arbitrarily scaled spectrum of molecular BPDT in H_2O (grey), and difference spectrum of spectra before and after linking (linked Au_{102} MPC - unlinked Au_{102} MPC, blue, scaled by factor 10).

This journal is © The Royal Society of Chemistry 20xx

Please do not adjust margins

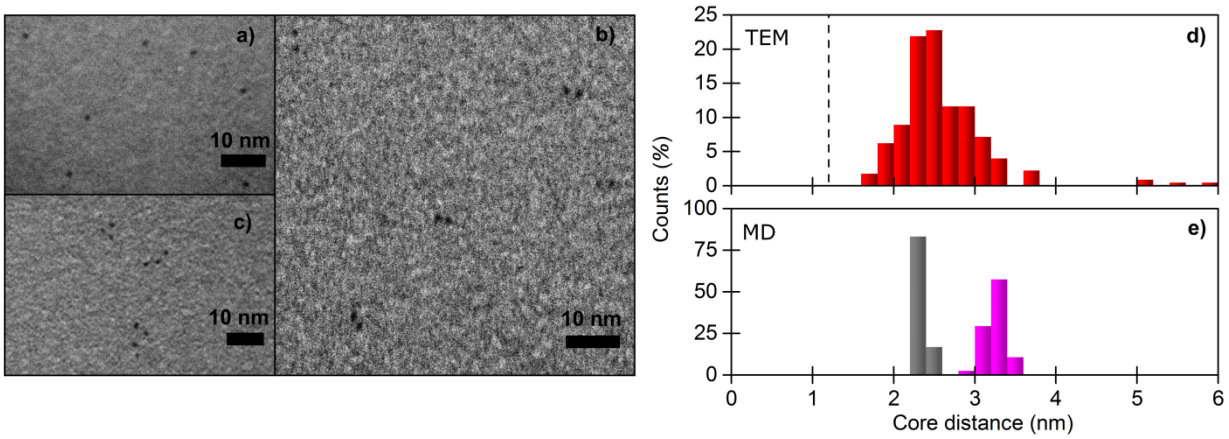

Fig. 5 TEM images of a) monomeric, b) dimeric, and c) trimeric Au_{102}MPCs in M, D, and T bands, respectively. Distribution of center-to-center distances of the linked Au_{102}MPC dimers d) from TEM images (number of particles, n = 220), and e) from simulation of fully-protonated (grey) and fully-deprotonated (purple) Au_{102}MPC – $(BPDT)_2$ – Au_{102}MPC in H_2O. The estimated core size of 1.2 nm is marked with a dashed vertical line.

X-ray structure[20] as described in Materials and Methods. The simulations were done in water both for the fully protonated and deprotonated forms of *p*-MBA ligand surface.

Simulations of the Au_{102}(*p*-MBA)$_{43}$-BPDT-Au_{102}(*p*-MBA)$_{43}$ dimer indicated that the linkage by a single BPDT is rather rigid and both sterically and electrostatically demanding. The deprotonated system was not stable unless electrostatic repulsion was screened by adding a significant amount of salt. The simulation in saline solution produced a very narrow center-to-center distance distribution between 2.5 – 2.7 nm (see Fig. S6A) that is unable to reproduce the full range of experimentally observed distances.

Simulations of Au_{102}(*p*-MBA)$_{43}$–$(BPDT)_2$–Au_{102}(*p*-MBA)$_{43}$ dimer with a disulfide bridge between the BPDT molecules indicated a stable and flexible system (see Fig. 6). The center-to-center distances started from 2.2 nm for the fully protonated system and extended up to 3.6 nm for the fully deprotonated systems, agreeing with the tails of the experimental distribution (see Fig. 5c). The simulated distributions of fully protonated and deprotonated clusters are relatively narrow and peak at the ends of the experimental spectrum. This suggests that Au_{102}MPCs are neither fully protonated nor fully deprotonated forming a distribution of distances based on the protonation level. Distances below 2.2 nm in the experimental distribution can be addressed to the roughness of the TEM support film leading to tilted dimers with respect to the imaging plane.

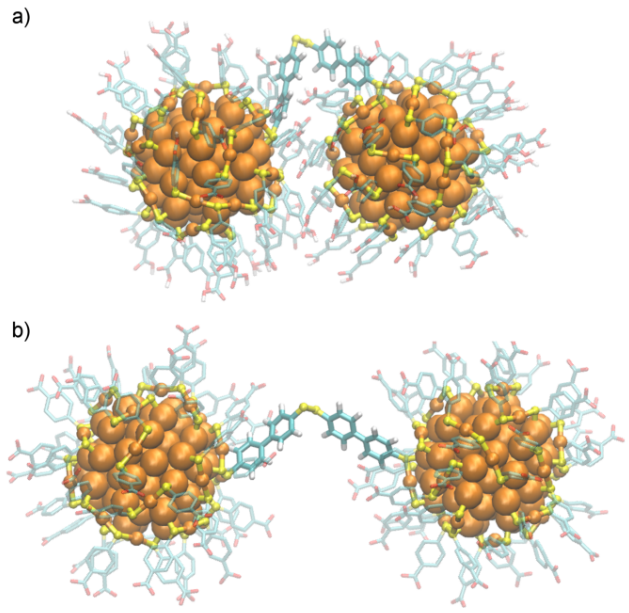

Fig. 6 Snapshot from MD simulation of a) fully protonated and b) fully deprotonated Au_{102}MPC – $(BPDT)_2$ – Au_{102}MPC in H_2O. Orange: Au; yellow: S; cyan, C; red: O. The disulfide bridge is highlighted by a yellow bond at the center.

Simulations of dimers, where three BPDT molecules connect fully deprotonated MPCs, yield a distribution which spans from 3.5 nm to 4.5 nm being above experimentally observed values (see ESI, Fig. S6E). Although, this does not exclude possibility of triple linker, it suggests that triple linking is rare. Dimers linked with multiple BPDT bridges are very unlikely due to low BPDT concentration used in the experiment (only two BPDT per 44 *p*-MBA). Therefore, the most straightforward explanation is that Au_{102}MPC dimers are linked primarily by two BPDT molecules with a single disulfide bridge between them.

Analysis of $Au_{\sim 250}$(*p*-MBA)$_n$ multimers. We did a similar PAGE analysis and separation for the crude product of $Au_{\sim 250}$(*p*-MBA)$_n$ ligand exchange reaction as for Au_{102}(*p*-MBA)$_{44}$. PAGE showed several distinct bands, however, the bands were less mobile than linked Au_{102}MPCs by a factor comparable to the mobility difference between unlinked MPCs (see Fig. 2, ESI Fig. S1). TEM imaging of the three lowest bands, M, D, and T, revealed dominantly monomeric, dimeric, and trimeric structures of $Au_{\sim 250}$(*p*-MBA)$_n$, respectively (see Fig. 7a-d and ESI, Figs. S7-9). The distributions of multimer core counts in M, D, and T bands in Fig. 7d were obtained from a concentrated sample prepared for UV-vis spectroscopy. The purity of the samples can be further increased by using less concentrated material in PAGE (see ESI, Figure S10).

Note that the D and T bands are very narrow, as in the case of Au_{102}(*p*-MBA)$_{44}$. This provides additional evidence that the $Au_{\sim 250}$(*p*-MBA)$_n$ is a monodisperse MPC.

Please do not adjust margins

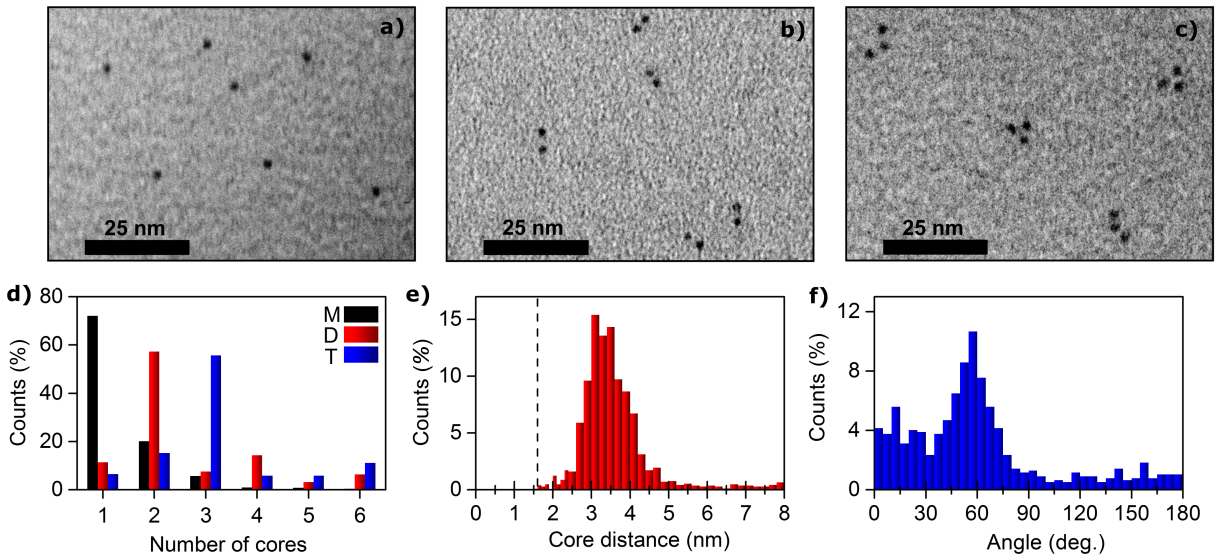

Fig. 7 TEM images of a) monomeric, b) dimeric, and c) trimeric $Au_{\sim 250}$MPCs. e) Statistics of multimers from M (number of particles, n = 1119), D (n = 227), and T (n = 624) bands of linked $Au_{\sim 250}$MPCs. Distribution of e) center-to-center distances for dimers (n = 1863), and f) angles for trimers (n = 770) analyzed from TEM images of linked $Au_{\sim 250}$MPCs. The estimated core size of 1.6 nm is marked with a dashed vertical line.

TEM analysis of center-to-center distances in the D band of $Au_{\sim 250}$MPCs was rather broad spanning from 2.6 nm up to 4.4 nm (see Fig 7e). The larger diameter of $Au_{\sim 250}(p\text{-MBA})_n$ adds a constant shift of 0.4 nm to the $Au_{102}(p\text{-MBA})_{44}$ distribution. The tail of the distribution extending up to 4.4 nm can be explained by contribution from dimers bound by three (or more) BPDT molecules. The larger electrostatic repulsion between $Au_{\sim 250}$MPCs compared to Au_{102}MPCs might favor longer linkers. Remarkably, the distribution of the angles in the TEM analysis of trimers showed a dominant peak at 60° indicating equilateral triangular multimers (see Fig. 7f), which is also clearly visible in the micrographs in addition to bent or linear geometries (see Fig. 7c, and ESI Fig. S9). The preference for equilateral triangles could be explained by a covalent bridge between each pair of MPCs in a trimer (see Fig. 1, and ESI, Fig S11).

Plasmon coupling in $Au_{\sim 250}(p\text{-MBA})_n$ multimers. To study optical properties of the plasmonic $Au_{\sim 250}(p\text{-MBA})_n$, we ran PAGE multiple times to prepare concentrated samples from M, D, and T bands. UV-vis absorption spectrum from the concentrated M band was equal to unlinked $Au_{\sim 250}(p\text{-MBA})_n$ in the visible region, but it showed changes in the UV region as in the case of Au_{102}MPCs. Comparison of spectra from M, D, and T bands, normalized to the main LSPR peak at 530 nm, (see Fig. 8a, and ESI, Figure S12) shows interesting new features for the linked $Au_{\sim 250}$MPCs in the visible region. The difference between normalized spectra of D and M bands (Fig. 8b) has two broad and significantly red-shifted peaks. These features become stronger in the difference spectrum between T and M bands. If we fit two Gaussian functions with an exponential background to the difference spectra, the fit reproduces these features extremely well in both cases. The obtained peak positions, 630 nm and 810 nm, are the same for the D and T bands. The features are weak compared to the main LSPR band, but they are locally significant altering absorption intensity up to ~10%. More importantly, they are reproducible (see ESI, Figure S13).

It is difficult to ascertain the origin of these modes experimentally. We observed, however, significant red-shift of the main LSPR peak when *unlinked* $Au_{\sim 250}$MPCs were agglomerated by reducing pH down to 3.5 (see ESI, Fig S14). This is typical plasmonic nanoparticle behavior which originates from the coupling of LSPR modes between nearby NPs.[3] The observed feature peaks at 635 nm in the difference

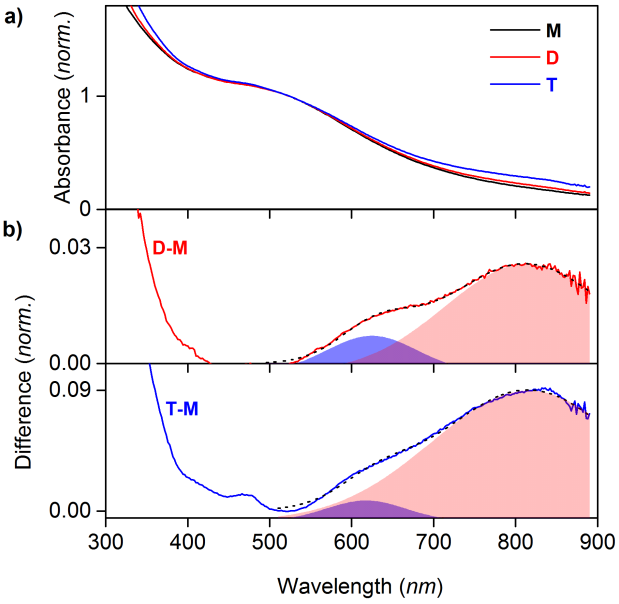

Fig. 8 a) Normalized UV-vis spectra of purified samples from M, D, and T bands. b) Difference spectra between samples from D and M bands (top) as well as from T and M bands (bottom). The shaded areas indicate Gaussian components found in the data and the dashed curves indicate the totals.

This journal is © The Royal Society of Chemistry 20xx

Please do not adjust margins

Please do not adjust margins

spectrum between low and high pH (see ESI, Fig S14). This strongly suggests that the peak at 630 nm in the spectra of $Au_{\sim 250}$MPC dimers and trimers originates from a coupled plasmon mode, called bonding dipolar plasmon (BDP) mode, where LSPRs of two nearby particles oscillate in-phase.[3] Therefore, this feature would not be directly related to the linker molecule, but only to the fact that two plasmonic particles are close to each other.

Using parameters relevant to our system (particle diameter 1.6 nm and edge-to-edge distance 1.4 nm), the well-known "plasmon ruler equation"[43] predicts a minor plasmon shift (< 10 nm) as compared to the observed shift of 100 nm from 530 nm to 630 nm. The failure of the plasmon ruler equation here could be due to its incompatibility to sub-2 nm MPCs for which atomistic details play an important role. The thickness of the ligand layer is comparable to the diameter of the metal core, and therefore, hybridization of the metallic core with the pi-electrons of the ligand layer might have significantly larger influence than in larger NPs.

We did not observe the peak at 810 nm in unlinked $Au_{\sim 250}$MPC agglomerates, and it is sensitive to the number of cores in the multimer. Therefore, we assign this mode to quantum-mechanical effects depending on the electronic structure of the molecular bridge. Previous studies of linked NPs have shown that a tunneling charge transfer plasmon (tCTP) can form between NPs when they are connected with a molecular linker or similar structure.[44-48] This mode typically exists together with the BDP mode, it is red-shifted with respect to the BDP mode, and it depends sensitively on the tunneling properties of the NP – molecule – NP junction. Moreover, tunneling through molecular states allows coupling over much longer distances than the normal charge transfer plasmon (CTP), that happens only over very short (< 1 nm) insulating gaps and causes blue-shift instead of red-shift[44,49,50]

Simulations of a simple two-level system between plasmonic NPs have showed that tCTP mode forms when a molecular state localized on the linker is near the Fermi level of the combined system.[47] To examine whether such localized states could exists in $Au_{\sim 250}$MPC multimers, we performed DFT simulations on a model system. While we do not have currently information of the atomic structure of $Au_{\sim 250}$MPC, we have previously done density functional theory (DFT) calculations on a slightly larger plasmonic $Au_{314}(SH)_{96}$ model MPC.[40] We now built a model system (see Fig. 9) by linking two such clusters via a disulfide-bridged BPDT pair and solved for its electronic structure using DFT. Several molecular states that are localized on BPDT were found starting 0.8 eV below (occupied states) and 1.7 eV above (unoccupied states) the Fermi level (see Fig. 9). These states are close enough to the Fermi level, that when coupled to LSPRs of MPCs in an optical

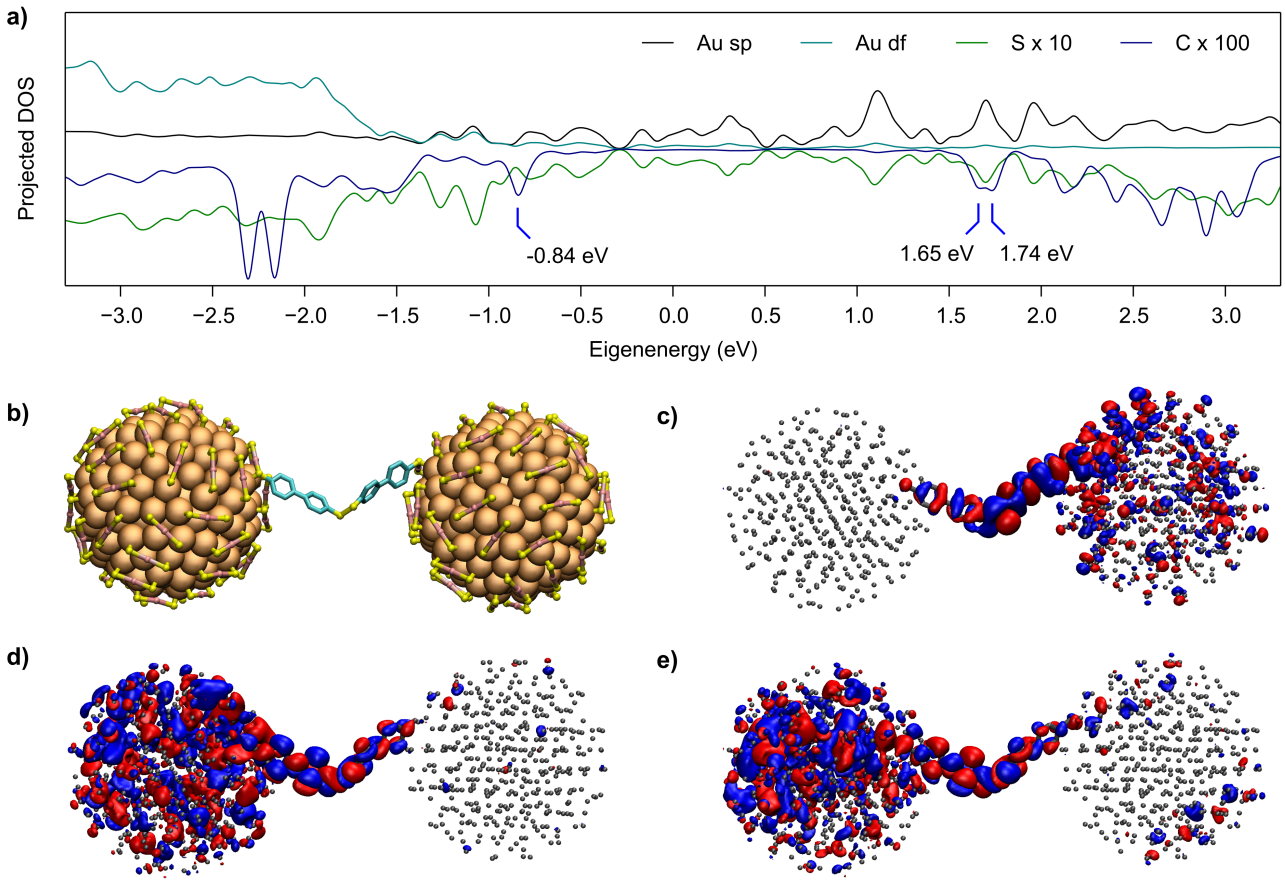

Fig. 9 a) Projected density of states for $Au_{314}(SH)_{95}$–BPDT–BPDT–$Au_{314}(SH)_{95}$ calculated using DFT. Projection to sulfur (green) is scaled by 10 and projection to carbon (blue) is scaled by 100 with respect to projection to s/p (black) and d/f (cyan) orbitals of gold. b) Geometry of $Au_{314}(SH)_{95}$–BPDT–BPDT–$Au_{314}(SH)_{95}$ dimer used in the calculation. Hydrogens are omitted for clarity. Isosurfaces for orbitals corresponding eigenenergies of c) -0.84 eV, d) 1.65 eV, and e) 1.74 eV with respect to the Fermi level.

Please do not adjust margins

Please do not adjust margins

excitation, they could act as tunneling channels for the tCTP mode, and therefore, account for the observed absorption in 700 - 900 nm range and possibly longer wavelengths.

Another possible explanation for the observed 810 nm peak is that the incoming BPDT ligand would alter the electronic structure of $Au_{\sim 250}(p\text{-MBA})_n$ and thus introduce new transitions near 800 nm. This is highly unlikely as the 810nm mode does not appear in the spectrum of $Au_{\sim 250}$MPC monomer or linked Au_{102}MPCs. Another BDP mode as the origin of 810 nm peak is also not plausible, because larger spectral red-shift would require shorter interparticle distance, which is not possible based on our MD simulations. All observations are in agreement with our proposed interpretation that the 810 nm peak originates from a tCTP or similar mode, nevertheless, further theoretical and experimental studies are needed to uncover the details of the plasmonic coupling in the linked $Au_{\sim 250}$MPC multimers.

Conclusions

We have achieved covalent linking between two gold nanoparticles which have a precisely known atomic structure, $Au_{102}(p\text{-MBA})_{44}$. In our approach, a BPDT molecule replaces a *p*-MBA ligand molecule in a ligand exchange reaction and becomes a part of the protecting ligand layer. The covalent disulfide bridge between two BPDT ligands joins the ligand layers and metal cores of two clusters forming a single unit with a well-defined atomic structure comparable to a molecule. This is an important step towards synthesis of atomically-precise MPC superstructures. Our approach differs from the previous studies, where linking has been noncovalent or atomic-level structure of the particle was unknown.

Moreover, we synthesized a larger, plasmonic monodisperse MPC, $Au_{\sim 250}(p\text{-MBA})_n$, and its multimers. Changes in the UV-vis spectra of $Au_{\sim 250}$MPC multimer indicated two hybridized LSPR modes with much larger red-shifts than expected from experiments of colloidal NPs. We assigned the first mode as the typical BDP mode in plasmonic NP aggregates. The second mode, however, is likely to originate from a tCTP, where tunneling happens through molecular states of disulfide bridged BPDT molecules. $Au_{\sim 250}$MPC multimers are the smallest systems reported which are essentially monodisperse, and show plasmonic coupling over a single covalently bound molecular bridge. Therefore, these systems are ideal candidates for connecting experimental observations to ab-initio level theory in the field of nanoplasmonics.

Acknowledgements

This work was financially supported by the Academy of Finland via projects 269402 and 273499 (L. L.), 265502 (E. H.), and 266492 (H. H.), The computations were made at the NSC and at CSC – the Finnish IT Center for Science in Espoo. We acknowledge Prof. T. Tsukuda, Assoc. Prof. K. Koyasu, Mr. K. Hirata for resources and support to measure mass spectrum in the University of Tokyo, during a visit (T.-R.T.) supported by the University of Jyväskylä. We acknowledge Drs. A. Johansson, G. Groenhof, P. Papponen, and Ms. E. Pohjolainen for technical help and Drs. X. Chen, J. Koivisto, S. Malola, and K. Salorinne for fruitful discussions.

Notes and references

1 U. Kreibig and M. Vollmer, Optical Properties of Metal Clusters, Springer-Verlag, Berlin Heidelberg, 1995.
2 C. Bréchignac, P. Houdy and M. Lahmani, Nanomaterials and Nanochemistry, Springer-Verlag Berlin Heidelberg, 2010.
3 N.J. Halas, S. Lal, W.S. Chang, S. Link and P. Nordlander, Chem. Rev., 2011, 111, 3913-3961.
4 C. Sönnichsen, B.M. Reinhard, J. Liphardt and A. P. Alivisatos, Nature Biotechnology, 2005, 23, 741-745.
5 B. M. Reinhard, M. Siu, H. Agarwal, A. P. Alivisatos and J. Liphardt, NanoLetters, 2005, 5, 2246-2252.
6 E. C. Le Ru and P. G. Etchegoin, Annu. Rev. Phys. Chem., 2012, 63, 65–87.
7 S. Yampolsky, D. A. Fishman, S Dey, E. Hulkko, M. Banik, E. O. Potma and V. A. Apkarian, Nature Photonics, 2014, 8, 650-656.
8 M. Quinten, U. Kreibig, D. Schönauer and L. Genzel, Surf. Sci., 1985, 156, 741-750.
9 X. Wang, G. Li, T. Chen, M. Yang, Z. Zhang, T. Wu and H. Chen, Nano Lett., 2008, 8, 2643-2647.
10 S.L. Kleinman, B. Sharma, M.G. Blaber, A.-I. Henry, N. Valley, R.G. Freeman, M.J. Natan, G.C. Schatz and R.P. Van Duyne, J. Am. Chem. Soc., 2013, 135, 301-308.
11 A. Cunningham, S. Mühlig, C. Rockstuhl and T. Bürgi, J. Phys. Chem. C, 2011, 115, 8955–8960.
12 C.L. Haynes and R.P. Van Duyne, J. Phys. Chem. B,, 2001, 105, 5599–5611.
13 S.J. Tan, M.J. Campolongo, D. Luo and W. Cheng, Nature Nanotechnol., 2011, 6, 268-76.
14 G.A. DeVries, M. Brunnbauer, Y. Hu, A.M. Jackson, B. Long, B.T. Neltner, O. Uzun, B.H. Wunsch and F. Stellacci, Science, 2007, 315, 358-361.
15 R. Sardar, T. Heap and J. S. Shumaker-Parry, J. Am. Chem. Soc., 2007, 129, 5356-5357.
16 H. Cha, J.H. Yoon and S. Yoon, ACS Nano, 2014, 8, 8554-8563.
17 T. Peterle, P. Ringler and M. Mayor, Adv. Funct. Mater., 2009, 19, 3497-3506.
18 D-H. Tsai, T. J. Cho, F. W. DelRio, J. M. Gorham, J. Zheng, J. Tan, M. R. Zachariah and V. A. Hackley, Langmuir, 2014, 30, 3397-3405.
19 T. Tsukuda, Häkkinen Häkkine and Protected H., Metal Clusters: From Fundamentals to Appliations, Elsevier, Amsterdam, 2015..
20 P.D. Jadzinsky, G. Calero, C.J. Ackerson, D.A. Bushnell and R.D. Kornberg, Science, 2007, 318, 430-433.
21 M. Walter, J. Akola, O. Lopez-Acevedo, P. D. Jadzinsky, G. Calero, C. J. Ackerson, R. L. Whetten, H. Grönbeck and H. Häkkinen, Proc. Natl. Acad. Sci., 2008, 105, 9157-9162.
22 C. L. Heinecke, T. W. Ni, S. Malola, V. Mäkinen, O. A. Wong, H. Häkkinen and C. J. Ackerson, J. Am. Chem. Soc., 2012, 134, 13316-13322.
23 S. Knoppe, A.C. Dharmaratne, E. Schreiner, A. Dass and T. Bürgi, J. Am. Chem. Soc., 2010, 132, 16783–16789.
24 S. Mustalahti, P. Myllyperkiö, S. Malola, T. Lahtinen, K. Salorinne, J. Koivisto, H. Häkkinen and M. Pettersson, ACSNano, 2015, 9, 2328–2335.
25 E. Hulkko, O. Lopez-Acevedo, J. Koivisto, Y. Levi-Kalisman, R.D. Kornberg, M. Pettersson and H. Häkkinen, J. Am. Chem. Soc., 2011, 133, 3752-3755.
26 C. Yi, H. Zheng, L. M. Tvedte, C. J. Ackerson and K. L. J. Knappenberger Jr., Phys. Chem. C, 2015, 119, 6307-6313.

 This journal is © The Royal Society of Chemistry 20xx

Please do not adjust margins

Please do not adjust margins

27 Y. Negishi, T. Nakazaki, S. Malola, S. Takano, Y. Niihori, W. Kurashige, S. Yamazoe, T. Tsukuda and H. Häkkinen, J. Am. Chem. Soc., 2015, 137, 1206-1212.
28 V. Marjomäki, T. Lahtinen, M. Martikainen, J. Koivisto, S. Malola, K. Salorinne, M. Pettersson and H. H. Häkkinen, Proc. Nat. Acad. Sci., 2014, 111, 1277-1281.
29 W.S. Compel, O.A. Wong, X. Chen, C. Yi, R. Geiss, H. Häkkinen, K.L. Knappenberger Jr. and C.J. Ackerson, ACS Nano, 2015, 9, 11690-11698.
30 K. Salorinne, T. Lahtinen, S. Malola, J. Koivisto and H. Häkkinen, Nanoscale, 2014, 6, 7823-7826.
31 Y. Levi-Kalisman, P.D. Jadzinsky, N. Kalisman, H. Tsunoyama, T. Tsukuda, D.A. Bushnell and R.D. Kornberg, J. Am. Chem. Soc., 2011, 133, 2976-2982.
32 K. Salorinne, S. Malola, O.A. Wong, C.D. Rithner, X. Chen, C.J. Ackerson and H. Häkkinen, Nature Communications, 2016, 7, 10401.
33 M. Azubel, J. Koivisto, S. Malola, D. Bushnell, G. L. Hura, A. H. Koh, H. Tsunoyama, T. Tsukuda, M. Pettersson, H. Häkkinen and R. D. Kornberg, Science, 2014, 345, 909-912.
34 B. Hess, C. Kutzner, D. van der Spoel and E. Lindahl, J. Chem. Theory Comput., 2008, 4, 435-447.
35 E. Pohjolainen, X. Chen, S. Malola, G. Groenhof and H. Häkkinen, J. Chem. Theory Comp., 2016, 12, 1342–1350.
36 M. D. Case, T. A. Darden, T. E., III Cheatham, C. L. Simmerling, J. Wang, R. E. Duke, R. Luo, R. C. Walker, W. Zhang, K. M. Merz, B. Roberts, S. Hayik, A. Roitberg, G. Seabra, J. Swails, A. W. Götz, I. Kolossváry, K. F. Wong, F. Paesani, J. Vanicek, R. M. Wolf, J. Liu, X. Wu, S. R. Brozell, T. Steinbrecher, H. Gohlke, Q. Cai, X. Ye, J. Wang, M. -J. Hsieh, G. Cui, D. R. Roe, D. H. Mathews, M. G. Seetin, R. Salomon-Ferrer, C. Sagui, V. Babin, T. Luchko, S. Gusarov, A. Kovalenko and P. A. Kollman, AMBER 12, University of California: San Fransisco, 2012..
37 M. Frisch, G. W. Trucks, H. B. Schlegel, G. E. Scuseria, M. A. Robb, J. R. Cheeseman, G. Scalmani, V. Barone, B. Mennucci, G. A. Petersson, H. Nakatsuji, M. Caricato, X. Li, H. P. Hratchian, A. F. Izmaylov, J. Bloino, G. Zheng, J. L. Sonnenberg, M. Hada, M. Ehara, K. Toyota, R. Fukuda, J. Hasegawa, M. Ishida, T. Nakajima, Y. Honda, O. Kitao, H. Nakai, T. Vreven, J. A., Jr. Montgomery, J. E. Peralta, F. Ogliaro, M. Bearpark, J. J. Heyd, E. Brothers, K. N. Kudin, V. N. Staroverov, R. Kobayashi, J. Normand, K. Raghavachari, A. Rendell, J. C. Burant, S. S. Iyengar, J. Tomasi, M. Cossi, N. Rega, J. M. Millam, M. Klene, J. E. Knox, J. B. Cross, V. Bakken, C. Adamo, J. Jaramillo, R. Gomperts, R. E. Stratmann, O. Yazyev, A. J. Austin, R. Cammi, C. Pomelli, J. W. Ochterski, R. L. Martin, K. Morokuma, V. G. Zakrzewski, G. A. Voth, P. Salvador, J. J. Dannenberg, S. Dapprich, A. D. Daniels, Ö. Farkas, J. B. Foresman, J. V. Ortiz, J. Cioslowski and D. J. Fox, Gaussian 09, Revision D.01, Gaussian Inc.: Wallingford CT, 2009..
38 C. I. Bayly, P. Cieplak, W. Cornell and P. A. Kollman, J. Phys. Chem., 1993, 97, 10269-10280.
39 J. Enkovaara, R. Rostgaard, J. J. Mortensen, J. Chen, M. Dulak, L. Ferrighi, J. Gavnholt, C. Glinsvad, V. Haikola, H. A. Hansen, H. H. Kristoffersen, M. Kuisma, A. H. Larsen, L. Lehtovaara, M. Ljungberg, O. Lopez-Acevedo, P. G. Moses, J. Ojanen, T. Olsen, V. Petzold, N. A. Romero, J. Stausholm, M. Strange, G. A. Tritsaris, M. Vanin, M. Walter, B. Hammer, H. Häkkinen, G. K. H. Madsen, R. M. Nieminen, J. K. Nørskov, M. Puska, T. T. Rantala, J. Schiøtz, K. S. Thygesen and K. W. Jacobsen, J. Phys.: Condens. Matter, 2010, 22, 253202.
40 S. Malola, L. Lehtovaara, J. Enkovaara and H. Häkkinen, ACS Nano, 2013, 7, 10263-10270.
41 G. Plascencia-Villa, B. Demeler, R. L. Whetten, W. P. Griffith, M. Alvarez, D. M. Black and M. Jose-Yacaman, J. Phys. Chem. C, 2016, 120, 8950-8958.
42 L.M. Tvedte and C.J. Ackerson, J. Phys. Chem. A, 2014, 118, 8124-8128.
43 P.K. Jain, W. Huang and M.A. El-Sayed, Nano Letters, 2007, 7, 2080-2088.
44 W. Zhu, R. Esteban, A. G. Borisov, J. J. Baumberg, P. Nordlander, H. J. Lezec, J. Aizpurua and K. B. Crozier, Nat. Comm., 2016, 7, 11495.
45 S.F. Tan, L. Wu, J.K.W. Yang, P. Bai, M. Bosman and C.A. Nijhuis, Science, 2014, 343, 1496-1499.
46 N. Zabala, O. Pérez-González, P. Nordlander and J. Aizpurua, Proc. SPIE, 2011, 8096, 80961L.
47 V. Kulkarni and A. Manjavacas, ACS Photonics, 2015, 2, 987–992.
48 T.P. Rossi, A. Zugarramurdi, M. J. Puska and R. M. Nieminen, Phys. Rev. Lett., 2015, 115, 236804.
49 K.I. Savage, M.M. Hawkeye, R. Esteban, A.G. Borisov, J. Aizpurua and J.J. Baumberg, Nature, 2012, 491, 574-577.
50 H. Jung, H. Cha, D. Lee and S. Yoon, ACS Nano, 2015, 9, 12292-12300.

This journal is © The Royal Society of Chemistry 20xx

Please do not adjust margins

Please do not adjust margins

Table of Contents

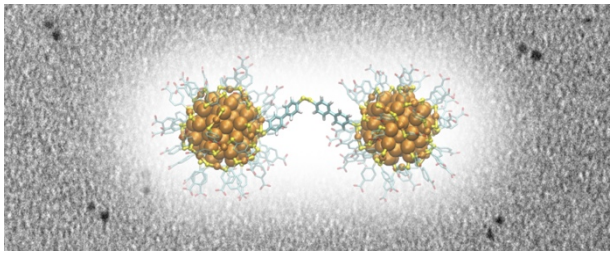

Covalently-linked multimers of monodisperse gold nanoclusters Au_{102}(*p*-MBA)$_{44}$ and $Au_{\sim 250}$(*p*-MBA)$_n$ were synthesized and plasmonic coupling was observed in $Au_{\sim 250}$(*p*-MBA)$_n$ multimers..

This journal is © The Royal Society of Chemistry 20xx

Please do not adjust margins